

Parametric analysis of modelling properties governing the seismic response of free-standing spent fuel racks

Alberto Gonzalez Merino

Equipos Nucleares S.A., Maliaño, Spain

University College Dublin, Dublin, Ireland

Luis Costas de la Peña

Equipos Nucleares S.A., Maliaño, Spain

Arturo González

University College Dublin, Dublin, Ireland

ABSTRACT: Spent fuel racks are steel structures designed to store the spent fuel assemblies removed from the nuclear power reactor. They rest in free-standing conditions submerged in the depths of the spent fuel pool. During a strong-motion earthquake, racks undergo large displacements subjected to inertial forces. An accurate estimation of their response is essential to achieve a safe pool layout and a reliable structural design. A transient analysis with direct integration of the equation of motion throughout the whole earthquake duration becomes therefore unavoidable. The computational cost associated to this analysis leads to the use of simplified finite element models giving rise to a certain dose of uncertainty. This paper carries out a parametric analysis of the key modelling properties for a two-rack system. This technique examines the behavior of the main transient outputs as a modelling parameter is systematically varied. Numerical results provide a source of insight into the general behavior of the rack system and an effective tool to propose an efficient and reliable modeling and meshing. The trade-off between outputs and computational cost and is also discussed.

1 INTRODUCTION

1.1 Description

Spent fuel racks are steel structures designed to store the spent fuel assemblies removed from the nuclear power reactor. In order to maximize the storage capacity of the spent fuel pool, rack units are spaced by only a few centimeters setting up a matrix shape that fits in the pool with a minimum clearance (Fig. 1). Rack units rest in free-standing conditions submerged in water at 12 m depth.

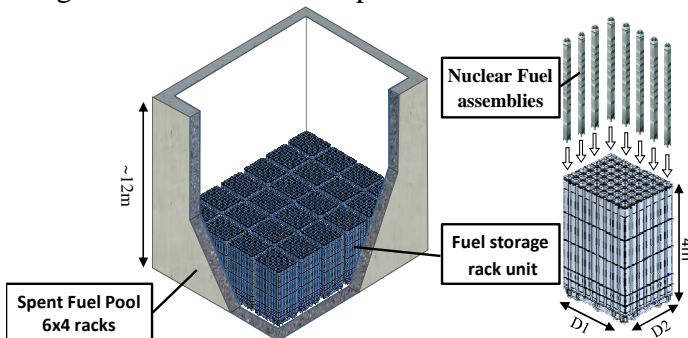


Figure 1. Location of free-standing racks in the spent fuel pool.

During a seismic event, racks undergo large displacements, namely sliding, rocking, twisting and turning with different types of possible impacts as fuel-to-rack, rack-to-rack and rack-to-pool. The rack support feet may lift off from or slide on the pool floor depending on the balance between inertial effects and friction resistance. Furthermore, the water

volume is also accelerated inducing a significant fluid-structure hydrodynamic interaction between the wet boundaries (Fritz 1972). The response of a unit is then influenced by the whole rack system due to the so-called ‘water coupling effect’ (Soler & Singh 1982)

1.2 Challenges in rack design

The seismic analysis is more complicated for the rack system than for most of other nuclear structural systems (Ashar & DeGrassi 1989, DeGrassi 1992). The United States Nuclear Regulatory Commission has issued overall design requirements and licensing acceptance criteria for the performance of these components (USNRC 1979, 1981). Their transient dynamic response is governed by their interaction with the surrounding fluid and exhibits a highly geometrical nonlinear behavior. The equation of motion associated to this problem need to be solved via numerical integration requiring significant computational power. An ad-hoc methodology based on the Finite Element (FE) method takes advantage of dynamic contact elements and implements the hydrodynamic mass concept (Dong 1978, Chung & Chen 1994). The latter has traditionally been accepted as a cost-effective approach to replace the water effect by an equivalent added mass. However, some dispersion of results still exists and several sources of uncertainty have been identified (Gonzalez et al. 2016a). In the following sections, a FE model of a

two-rack system is introduced and the influence of key modelling parameters on the transient response and on the computational time is assessed. Analyses are performed on ANSYS Mechanical APDL Release 14.0 running in an Intel core i3 processor with 8GB RAM.

2 CONCEPTUAL MODEL FOR 3D SEISMIC ANALYSIS

The computational cost of the aforementioned non-linear dynamic time history analysis has motivated the use of plain but efficient models (Soler & Singh 1984, Zhao et al. 1996, Zhao 1997, Hinderks et al. 2001). Figure 2 shows an upgrade of the 2-rack stick model used by Gonzalez et al. (2016b) to simulate the response of free-standing racks. Such a model allows for the sliding and rocking motion and takes into consideration the geometric nonlinearities associated to the dynamic contacts (i.e. fuel rattling inside the storage cells, tilting uplifts of support feet and subsequent impacts, frictional sliding of the support feet along the pool liner, etc.).

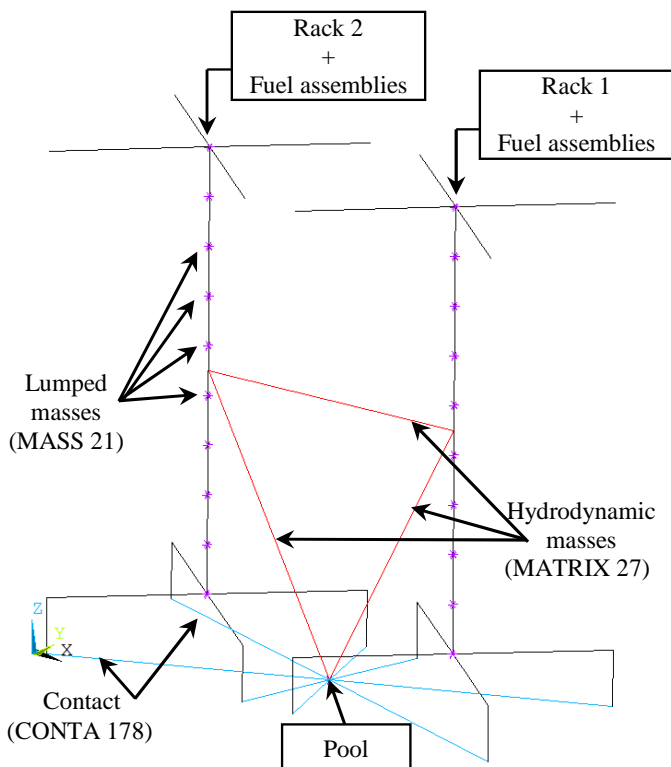


Figure 2. Seismic 3D ANSYS FE model of 2-rack system

The model is built in 3D in order to reproduce the real spatial motion which cannot be achieved by a planar approach. Each rack unit is composed by 4 feet connected to four rigid beams forming a pedestal that serves as support to a vertical beam representing the storage cells at the body of the rack. Beam elements are massless and defined with a specific stiffness to replicate the genuine dynamic behavior. Rack and fuel masses are lumped into mass elements MASS21 at different levels whereas their self-weight are input as a force on their centroid. MATRIX27 elements modify the effective masses

according to the hydrodynamic mass concept to take into account the fluid-structure interaction of the water coupling effect. CONTA178 elements simulate the dynamic contact and friction forces caused by the rocking and sliding motion.

Regarding the fuel assemblies, they are assumed to move in phase. They can therefore be grouped and modeled using a single fuel beam collinear with the rack body beam (i.e. labelled 'rack + fuel assemblies' in the figure). Nodes of the fuel beam are connected to the nodes of the rack body beam at each discretization level through both cylindrical contacts CONTA178 and dynamic fluid coupling elements FLUID38. The former recreate contact impact forces in the radial direction and Coulomb friction in the tangential direction. The latter simulate the effect of the constrained mass of water encompassed between the fuel assembly and the storage cell (Stabel & Ren 2001)

3 ACCELERATION INPUT

External seismic load is usually given in the form of design response spectra from which a synthetic acceleration time history can be derived using the PSD method. Figure 3 illustrates the horizontal acceleration-time history used in this parametrical analysis. It lasts around 12 seconds and exceeds 8m/s^2 .

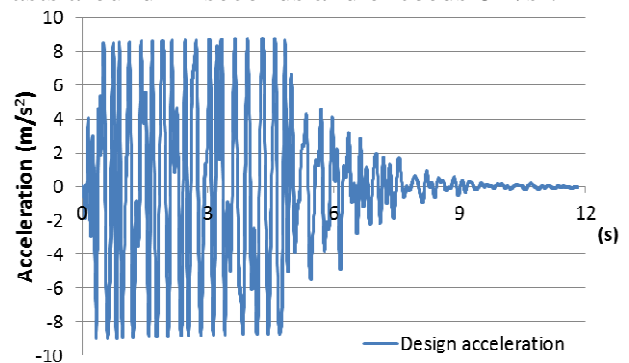


Figure 3. Design acceleration-time history

Since in primitive FE programs accelerations could not be directly applied to the model some alternatives were developed to enforce the pool to reproduce this accelerogram. Lee et al. (1998) advised against the use of the displacement-time history in the typical sharp accelerograms of the rack seismic analysis. This scheme results in unexpected acceleration discontinuities throughout the simulation bringing numerical noise that can only be limited through numerical damping.

Thenceforth, transient accelerations have traditionally been transformed into an equivalent force pushing a huge 'ground' mass. This force-time history is set as the product of the ground mass by the acceleration at each time step. The ground mass has to be some orders of magnitude bigger than the mass of the rack system in order to reduce their influence. Unfortunately, this requirement may introduce a loss of

computational accuracy due to the combination of large and small numbers. Moreover, since this scheme computes the accelerations terms via the solution of the complete differential equation of motion, it adds computational time and results in slight differences between the design and computed acceleration. The magnitude of the error depends on the solution of the 2nd order ODE and then on the time marching.

Figure 4 compares the total and relative acceleration error in a typical transient analysis for a time step of 3e-5 seconds. Total error is the difference (i.e. design - computed) and relative error is the ratio expressed as a percentage (i.e. 1-(computed / design)). It is noted that even if the total error remains low and bounded in the order of 4e-2 m/s², the percentage can reach peaks up to 1400% during the shakings.

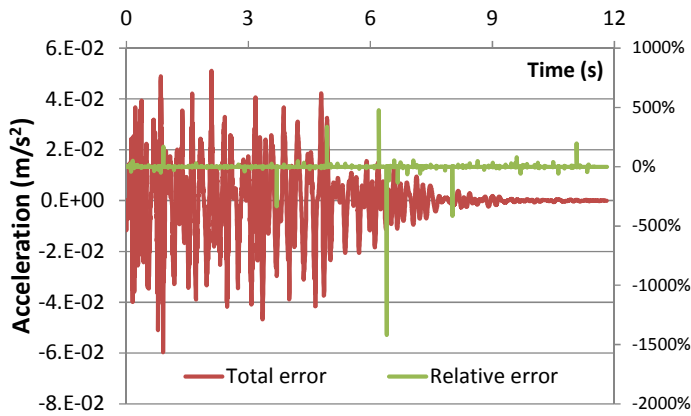


Figure 4. Total and relative errors in the computation of the pool acceleration when input as an equivalent force.

This computation error can be overcome by using FE programs that allow the user to directly feed the design acceleration into to the model. For instance, ANSYS recommends to define support motion using the tabular array parameter definition on the ‘D,,acc’ command (QA2012-01, 2012). Figure 5 shows how the total and relative acceleration error disappears when the same analysis is conducted with a directly enforced acceleration-time history. The remaining error is due to the last significant digit of the result output.

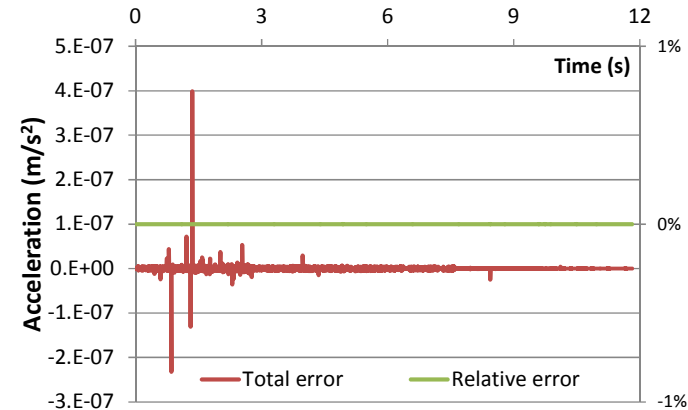


Figure 5. Total and relative errors in the computation of the pool acceleration when input as an enforced acceleration.

4 FINITE ELEMENT MESH DISCRETIZATION

4.1 Rack body beam

The continuous model is discretized into finite elements that can be addressed through computational analysis. The 4m height of the rack body is divided into several levels (n_{levels}). Each level is represented by a node where structural lumped mass, hydrodynamic added mass and fuel contact and dynamic fluid coupling are set. The total mass of the rack ($M_{rack}=630$ kg) is lumped proportionally to the span of each level. A $M_{rack}/(n_{levels}-1)$ mass is assigned to the central nodes, whereas a $M_{rack}/(n_{levels}-1)/2$ mass is assigned to the bottom and top nodes. Hydrodynamic added masses resulting from the racks underwater relative acceleration are geometrically split into the number of levels through constraint equations.

4.2 Fuel assemblies beam

The total mass of the fuel assemblies ($M_{fuel}=2500$ kg) is also lumped proportionally to the span of each level. While a mass of value $M_{fuel}/(n_{levels}-1)$ is assigned to central nodes, $M_{fuel}/(n_{levels}-1)/2$ is assigned to the end nodes.

4.3 Parametric analysis of the FE mesh discretization

During the transient analysis the equation of motion is solved at each node at each time step to satisfy equilibrium. Therefore, the computational cost is proportional to number of nodes. A parametric analysis of the FE mesh is carried out to highlight not only its influence on the CPU time but also on crucial design outputs as displacements and forces. Several runs have been performed on variations of the model of Figure 2 for different meshes with n_{levels} ranging from values 2 to 50. Figure 6 compares the relative sliding displacement of the Rack1 over the pool floor throughout the transient analysis. Table 1 provides the bounds of most interest for design purposes and Figure 7 shows the sensitivity of these outputs to the FE mesh discretization.

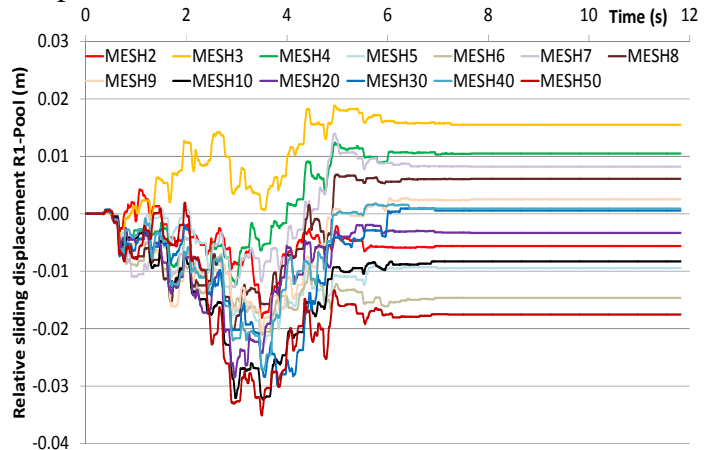


Figure 6. Relative sliding displacements Rack1 - Pool for different FE meshes

Table 1. Mesh discretization versus CPU time and output bounds

Number of levels	CPU time	Max. relative sliding displacement	Min. relative sliding displacement	Max. Vertical force on support
n_{levels}	(s)	(cm)	(cm)	(N)
2	3.81E3	0.43	-1.81	8.05E4
3	4.24E3	1.88	-0.44	9.46E4
4	4.51E3	1.37	-0.91	1.14E5
5	4.73E3	0.21	-2.28	1.37E5
6	5.08E3	0.03	-2.10	1.04E5
7	5.48E3	1.39	-1.28	1.15E5
8	5.97E3	0.68	-2.03	1.16E5
9	6.16E3	0.28	-2.04	1.13E5
10	6.69E3	0.06	-3.24	1.16E5
20	1.17E4	0.06	-2.84	1.16E5
30	1.76E4	0.10	-2.98	1.18E5
40	2.40E4	0.06	-5.52	1.01E5
50	2.90E4	0.19	-3.51	1.19E5

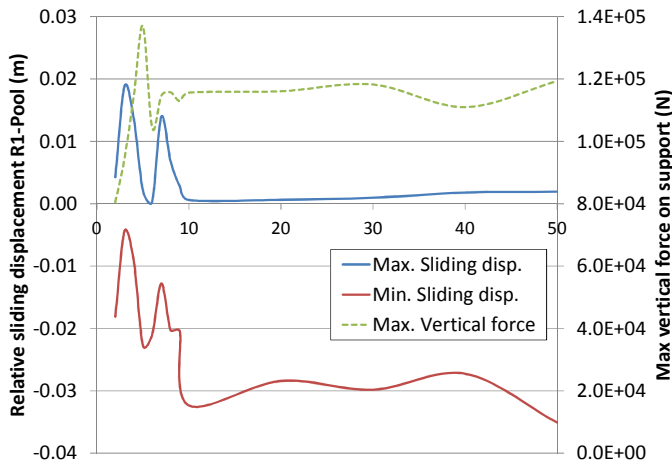


Figure 7. Sensitivity of the sliding displacement and maximal vertical force to the mesh discretization

It is noted that the maximum and minimum sliding displacements are affected by the number of levels of the mesh. Models with less than 10 levels present a wide dispersion in the outputs whereas models exceeding 10 levels present stabilized sliding displacements and forces and are definitely more reliable. Regarding the CPU time, it increases linearly with the number of nodes in an average of 525 s. per extra level.

5 FRICTION COEFFICIENT

The friction coefficient at the contact between the rack feet and the pool liner has a strong influence in the relative sliding motion. Low frictions are associated to high sliding displacements whereas high frictions lead to a foremost rocking behavior boosting the vertical forces associated to the impacts on supports. Several runs have been performed on the model of Figure 2 for different values of the Coulomb friction coefficient ranging from 0.2 to 0.8 (Rabinowicz 1976). Figure 8 compares the relative sliding displacement of the Rack1 over the pool floor throughout the transient analysis. Table 2 provides the bounds of most interest for design purposes and Figure 9 shows the sensitivity of these outputs to the friction coefficient.

vides the bounds of most interest for design purposes and Figure 9 shows the sensitivity of these outputs to the friction coefficient.

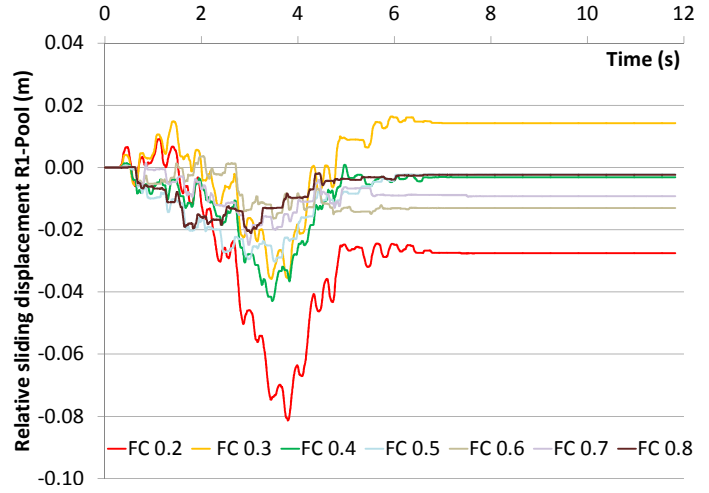


Figure 8. Relative sliding displacements Rack1 - Pool for different friction coefficients (FC)

Table 2. Friction coefficient versus CPU time and output bounds

Friction coeff.	CPU time	Max. relative sliding displacement	Min. relative sliding displacement	Max. Vertical force on support
	(s)	(cm)	(cm)	(N)
0.20	7.02E3	0.92	-8.13	4.04E4
0.30	7.24E3	1.63	-3.58	6.35E4
0.40	6.88E3	0.13	-4.28	8.84E4
0.50	6.62E3	0.06	-3.03	1.10E5
0.60	6.22E3	0.36	-1.65	9.91E4
0.70	6.20E3	0.10	-2.49	1.10E5
0.80	6.14E3	0.01	-2.11	9.44E4

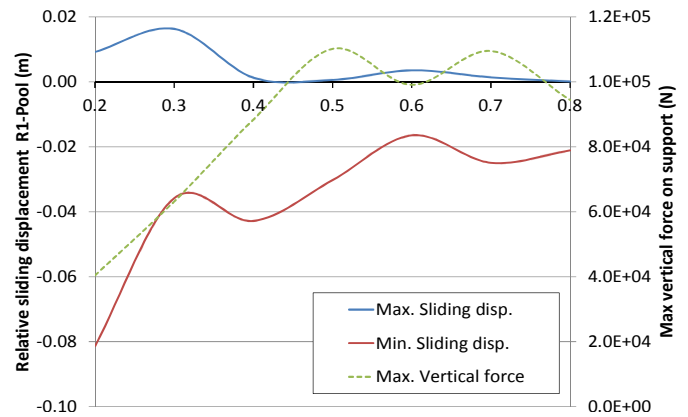


Figure 9. Sensitivity of the sliding displacement and maximal vertical force to the friction coefficient

In Figure 9, the area between the blue and red line (i.e. max and min displacements) represents the maximal amplitude of the sliding displacement around the initial position. It is noted that this amplitude strongly decreases between 0.2 and 0.6, and then it remains quasi constant between 0.6 and 0.8. A similar pattern is observed for the vertical force going from the 'sliding domain' to the 'rocking domain'. It increases with the friction for coefficients up to 0.5, and then it gets stabilized.

6 RACK-TO-POOL CONTACT STIFFNESS

The stiffness of the contact between the rack feet and the pool liner determines the roughness of the impacts. Several runs have been performed on the model of Figure 2 for different values of the contact stiffness ranging from $1e6$ to $1e12$ N/m. Figure 10 compares the relative sliding displacement of the Rack1 over the pool floor throughout the transient analysis. Table 3 provides the bounds of most interest for design purposes and Figure 11 shows the sensitivity of these outputs to the rack-to-pool contact stiffness.

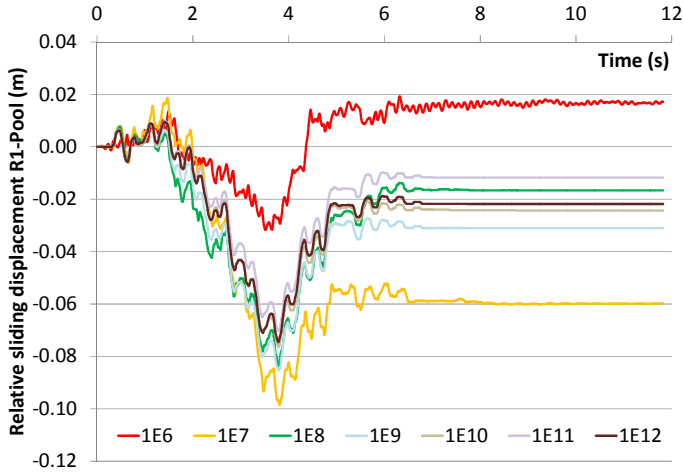


Figure 10. Relative sliding displacements Rack1 - Pool for different rack-to-pool contact stiffness

Table 3. Rack-to-pool contact stiffness versus CPU time and output bounds

Contact stiffness	CPU time	Max. relative sliding displacement	Min. relative sliding displacement	Max. Vertical force on support
(N/m)	(s)	(cm)	(cm)	(N)
1E6	5.85E3	1.93	-3.17	8.66E3
1E7	6.16E3	1.87	-9.85	1.76E4
1E8	6.39E3	0.86	-8.39	3.46E4
1E9	7.10E3	0.90	-8.53	4.22E4
1E10	8.72E3	0.94	-7.64	1.23E5
1E11	1.03E4	0.99	-7.04	1.66E5
1E12	1.52E4	0.95	-7.45	2.10E5

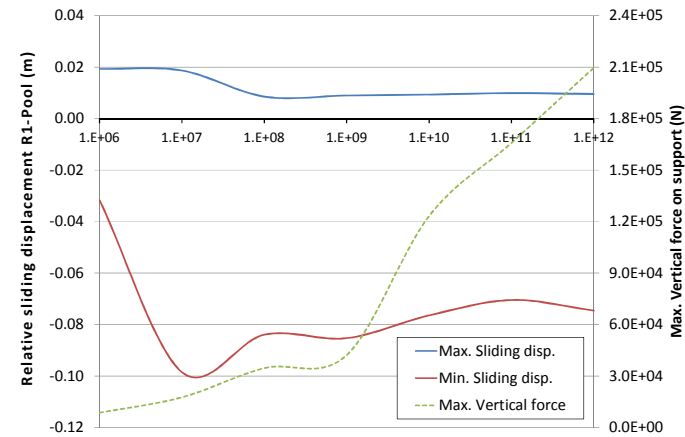


Figure 11. Sensitivity of the sliding displacement and maximal vertical force to the rack-to-pool contact stiffness.

In general, the overall displacements are barely influenced by the stiffness of the rack-to-pool contact. However, it is noted that stiffer contacts cause sharper impacts leading to greater peaks on the vertical forces on supports. In addition, since sharp impacts represent a convergence problem a reduction in the time steps throughout the contact event is required which increases the computational cost.

7 FUEL-TO-CELL CONTACT STIFFNESS

Fuel assemblies rattle inside the storage cells following to the rack shakings. This secondary-body motion contributes to the rocking behavior since fuel-to-cell impacts are eccentric as they firstly happen on the very top of the rack body. The stiffness of the contact between the fuel and the cell determines the roughness of the impacts, and therefore the way the kinetic energy is transmitted. Several runs have been performed on the model of Figure 2 for different values of the contact stiffness ranging from $1e4$ to $1e10$ N/m. Figure 12 compares the relative sliding displacement of the Rack1 over the pool floor throughout the transient analysis. Table 4 provides the bounds of most interest for design purposes and Figure 13 shows the sensitivity of these outputs to the fuel-to-cell contact stiffness.

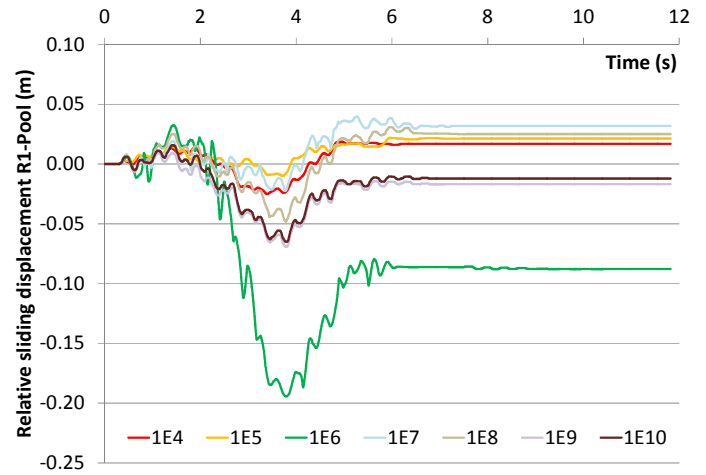


Figure 12. Relative sliding displacements Rack1 - Pool for different fuel-to-cell contact stiffness

Table 4. Fuel-to-cell contact stiffness versus CPU time and output bounds

Contact stiffness	CPU time	Max. relative sliding displacement	Min. relative sliding displacement	Max. Vertical force on support
(N/m)	(s)	(cm)	(cm)	(N)
1E4	5.25E3	1.86	-2.51	9.53E3
1E5	6.31E3	2.18	-0.98	9.55E3
1E6	8.17E3	3.25	-19.42	1.52E5
1E7	7.69E3	3.96	-2.24	6.76E4
1E8	7.19E3	3.09	-4.83	4.88E4
1E9	7.17E3	0.91	-6.94	4.04E4
1E10	7.29E3	1.57	-6.51	3.98E4

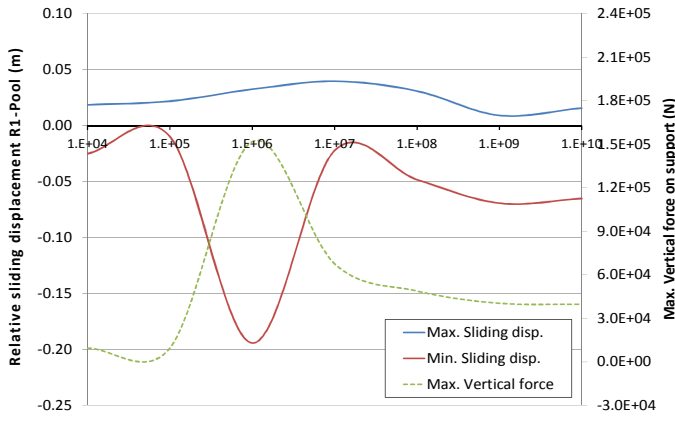


Figure 13. Sensitivity of the sliding displacement and maximal vertical force to the fuel-to-cell contact stiffness.

As mentioned in the previous section, the computational cost increases with the stiffness of the contact due to the convergence difficulties that require smaller time steps. In addition, it is noted here an important resonance effect when the contact stiffness approach $1E6$. Around this value, sliding displacement and forces are boosted.

8 GAP BETWEEN THE FUEL ASSEMBLY AND THE STORAGE CELL

The gap existing between the fuel assembly and the storage cell determines the magnitude and recurrence of the impacts. It limits the oscillation amplitude, and therefore the maximal relative velocity reachable by assemblies before impact as well as the damping action of the encompassed water damps the motion. In general, small gaps mean frequent minor impacts, whereas larger gaps lead to rare but stronger impacts forces due to bigger inertial effects of the fuel mass. Several runs have been performed on the model of Figure 2 for different values of the gap ranging from 2 to 14 mm. Figure 14 compares the relative sliding displacement of the Rack1 over the pool floor throughout the transient analysis. Table 5 provides the bounds of most interest for design purposes and Figure 15 shows the sensitivity of these outputs to the fuel gap.

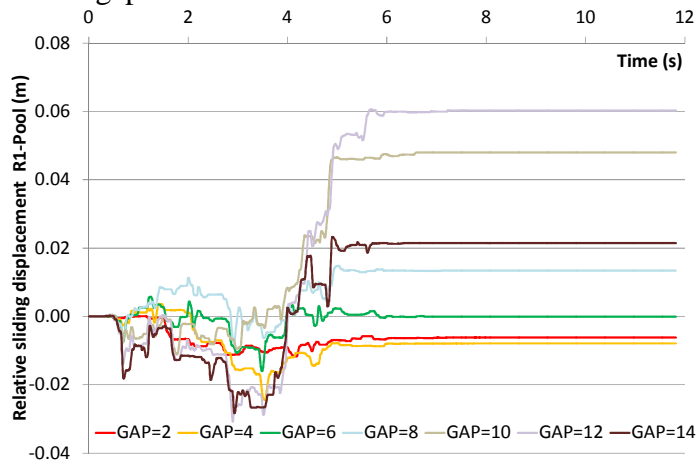


Figure 14. Relative sliding displacements Rack1-Pool for different fuel gaps

Table 5. Fuel gap versus CPU time and output bounds

Gap	CPU time	Max. relative sliding displacement	Min. relative sliding displacement	Max. Vertical force on support
(mm)	(s)	(cm)	(cm)	(N)
2	6.54E3	0.00	-1.17	8.10E4
4	6.45E3	0.37	-2.44	8.85E4
6	6.63E3	0.58	-1.60	1.16E5
8	6.49E3	1.48	-0.79	1.21E5
10	6.62E3	4.80	-1.11	1.03E5
12	6.68E3	6.06	-3.08	1.02E5
14	6.73E3	2.33	-2.83	1.14E5

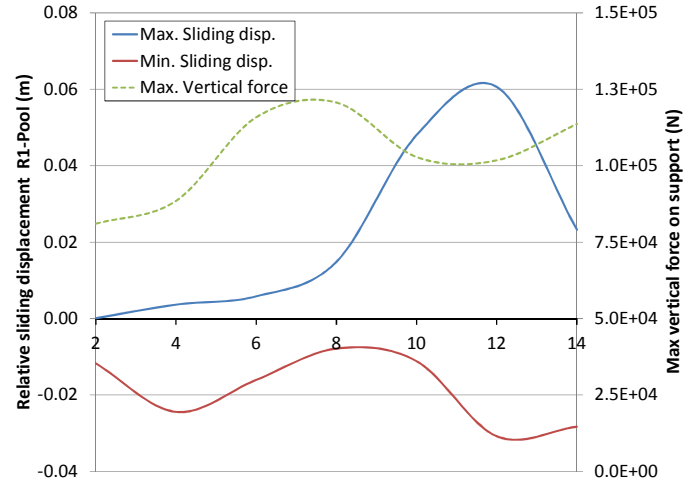


Figure 15. Sensitivity of the sliding displacement and maximal vertical force to the fuel gaps

It is noted that the CPU usage is unaffected by the variation in the gap thickness. In the same way, sliding displacements are barely affected when gaps remains small, varying between 2 and 8mm. However, they experience a big magnification when gaps exceed 8mm and fuel assemblies can oscillate more freely.

9 FLEXURAL RIGIDITY OF THE FUEL ASSEMBLY

The flexural rigidity of the fuel assembly represents the ability of the fuel assembly to deform after the impacts. It influences the roughness of the impacts and determines somehow the number of contacts activated along the fuel beam at each shaking. Rigid assemblies only impacts on the end nodes, whereas soft assemblies deforms up to stick to the cell walls. Several runs have been performed on the model of Figure 2 for different values of the flexural rigidity ranging from $2E0$ to $2E6$ N.mm². Figure 16 compares the relative sliding displacement of the Rack1 over the pool floor throughout the transient analysis. Table 6 provides the bounds of most interest for design purposes and Figure 17 shows the sensitivity of these outputs to the fuel flexural rigidity.

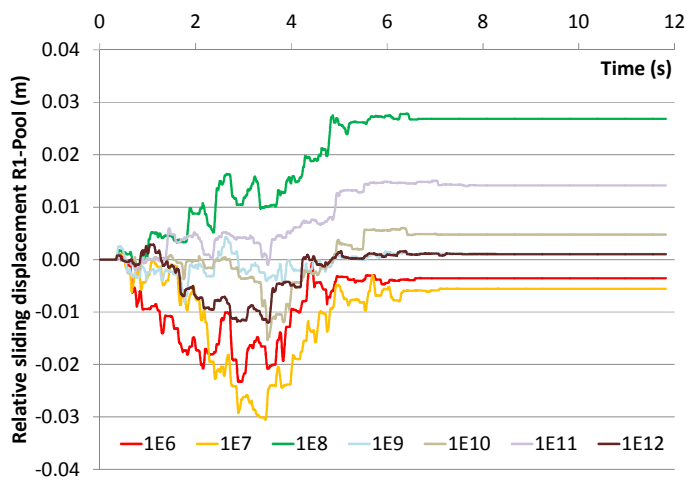


Figure 15. Relative sliding displacements Rack1-Pool for different fuel flexural rigidity

Table 6. Fuel flexural rigidity versus CPU time and output bounds

EI	CPU time	Max. relative sliding displacement	Min. relative sliding displacement	Max. Vertical force on support
(N.m ²)	(s)	(cm)	(cm)	(N)
2E0	7.53E3	0.28	-1.20	8.28E4
2E1	7.56E3	1.50	-0.21	1.06E5
2E2	7.03E3	0.60	-1.54	1.11E5
2E3	6.61E3	0.43	-0.82	8.39E4
2E4	6.52E3	2.78	-0.19	8.11E4
2E5	6.81E3	0.11	-3.05	1.01E5
2E6	6.82E3	0.07	-2.33	1.11E5

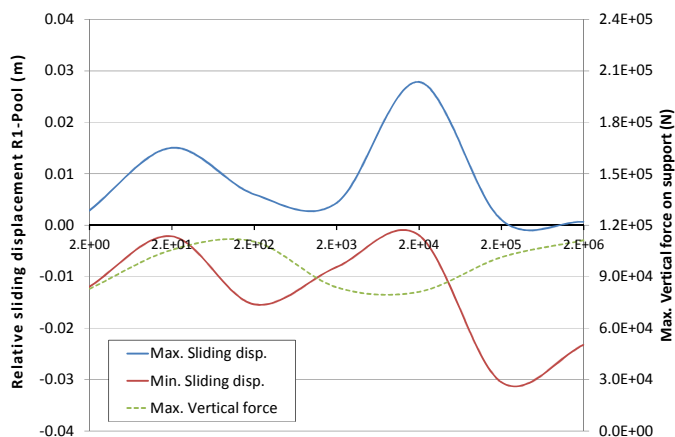


Figure 16. Sensitivity of the sliding displacement and maximal vertical force to the fuel flexural rigidity

It is noted that the general behavior of the rack unit in terms of sliding amplitude and vertical force is scarcely affected. Moreover, only slight variations in the CPU usage are founded.

10 RESULTS AND DISCUSSION

The seismic behavior of the rack systems is very complex and somehow chaotic. Any slight divergence in the initial steps causes a visible effect in the final results of the transient analysis. Minor variations in the modelling parameters lead to a wide de-

viation in final results. Nevertheless, the following relevant conclusions can be drawn from the parametrical analysis of this 2-rack system:

- a transient analysis with enforced acceleration-time history is recommended to avoid acceleration discontinuities,
- a 10 levels mesh discretization provides stable results within a limited computation time so it is considered cost effective,
- sliding displacements are strongly influenced by the friction coefficient, especially in the range of 0.2 to 0.6,
- very stiff rack-to-pool contacts lead to a safe structural design since the peaks of vertical force on supports are maximized,
- a resonance effect can happen in the fuel rattling and the rack rocking in function of fuel-to-cell contact stiffness,
- an influence of fuel gaps in the sliding displacements is only visible for gaps larger than 8 mm,
- flexural rigidity has slight influence in the general behavior of the rack unit.

11 ACKNOWLEDGEMENTS

This project has received funding from the European Union's Horizon 2020 research and innovation programme under the Marie Skłodowska-Curie grant agreement No. 642453 (<http://trussitn.eu>)



REFERENCES

- ANSYS, Inc. 2012. *ANSYS QA2012-01*
- ANSYS, Inc. 2013. *ANSYS Mechanical User's guide: Release 15.0*
- Ashar, H. & DeGrassi, G. 1989. Design and analysis of free-standing spent fuel racks in nuclear power plants (an overview). *10th International Conference on Structural Mechanics in Reactor Technology, SMiRT; CONF-890855—43, BNL-NUREG-42667.*
- Chung, H., & Chen, S. (1994). Hydrodynamic mass, CONF-840647—9, United States Government,
- DeGrassi, G. Review of the technical basis and verification of current analysis methods used to predict seismic response of spent fuel storage racks, NUREG/CR-5912, BNL-NUREG-52335. 1992.
- Dong, R.G. 1978. *Effective mass and damping of submerged structures.* Lawrence Livermore laboratory UCRL-52342.
- Fritz, R.J. 1972. The effect of liquids on the dynamic motions of immersed solids. *Journal of engineering for industry;* 167-173
- Gonzalez, A., Costas, L., Gonzalez, A. 2016a. Uncertainties in seismic design of free-standing HDSFS racks. *International Youth Nuclear Congress (IYNC).*
- Gonzalez, A., Costas, L., Gonzalez, A. 2016b. Dynamic analysis of the nonlinear response of high density fuel storage racks. *Civil Engineering Research in Ireland (CERI)*
- Hinderks, M., Ungoreit, & H., Kremer G. 2001 Improved method to demonstrate the structural integrity of high density fuel storage racks. *Nuclear engineering and design,* 206, 177-184.

- Lee, G.M., Kim, K.S., Park, K.B., Park, J.K. 1998. Three-dimensional seismic analysis for spent fuel storage rack. *Journal of the Korean Nuclear Society*: 30:91-98.
- Rabinowicz, E. 1976. *Friction coefficients of water-lubricated stainless steel for a spent fuel rack facility*. Massachusetts Institute of Technology, a report for Boston Edison company.
- Soler, A., & Sing K. 1984. Seismic response of a free standing fuel rack construction to 3-D floor motion. *Nuclear engineering and Design*, 80, 315-329.
- Soler, A.I., Singh, K.P. 1982. Dynamic coupling in a closely spaced two-body system vibrating in a liquid medium: the case of fuel racks, *3rd Keswick International conference in nuclear plants*.
- Stabel, J. & Ren, M. 2001. Fluid-Structure interaction for the analysis of the dynamics of fuel storage racks in the case of seismic loads. *Nuclear Engineering and Design*: 206:167-176.
- U.S. Nuclear Regulatory Commission. 1978. OT position for review and acceptance of spent fuel storage and handling applications. Amended by NRC letter in 1979
- U.S. Nuclear Regulatory Commission. 1981. *Standard Review Plan for the review of safety analysis reports for nuclear power plants*. Chapter 3– Design of structures, components, equipment and systems. NUREG-0800, formerly issued as NUREG-75/087.
- Zhao, Y. 1997. Finite element modelling and analysis of non-linear impact and frictional motion response including fluid-structure coupling effects. *Shock and vibration*: 4:311-325.
- Zhao, Y., Wilson, P.R. Stevenson, J.D. 1996. Nonlinear 3-D dynamic time history analysis in the rerecking modification for a nuclear power plant. *Nuclear Engineering and Design*: 165:199-221.